Composites Science and Technology 182 (2019) 107750

Contents lists available at ScienceDirect

Composites Science and Technology

journal homepage: www.elsevier.com/locate/compscitech

Snap-through and stiffness adaptation of a multi-stable Kirigami composite module

Aditya Lele, Vishrut Deshpande, Oliver Myers, Suyi Li*

Department of Mechanical Engineering, Clemson University, Clemson, SC, USA

ARTICLE INFO

Keywords:
Bistable composite
Kirigami
Snap-through instability
Variable stiffness

ABSTRACT

Multi-stable composite laminates have been used to create adaptive and shape-morphing structures for many applications. However, it remains challenging to use these composites to obtain complicated shape changes and mechanical property adaptations. This study proposes a "Kirigami composite" concept to help address this challenge. By strategically placing slit cuts into the composite laminate with carefully designed fiber layout, one can release the internal constraints and significantly enrich the achievable shapes and adaptive functions. This study focuses on the elementary Kirigami composite module consisting of a single slit cut and two bistable patches. Experiments and finite element simulations show that this Kirigami module exhibits four different stable equilibria and its snap-through instability originates from a rapid "run-away" growth of surface curvature inversions due to connecting tab. This study also investigates a stiffness adaptation function. These results can be used for creating more sophisticated Kirigami composite structures with multiple patches and cuts.

1. Introduction

Thin composite laminates with an asymmetric fiber layout can develop a multi-stability due to the non-uniform residual stress developed in the curing process [1,2]. These laminates possess at least two stable equilibria (or stable states) so that when they are deformed to a critical configuration, an elastic instability would occur and rapidly deform the laminates towards a distant stable state. This process is typically known as the "snap-through". Harnessing such multi-stability and snap-through has yielded a wide spectrum of adaptive functionalities [3]. Shape morphing is the most extensively analyzed example. Multi-stable composites have several advantages that make them uniquely attractive for such a purpose: i) they need no constant power supply to maintain their shapes at stable states; ii) the snap-through typically features a large deformation and short response time, and iii) fiber composites inherently have high stiffness and strength-to-density ratios. As such, multi-stable composites have been investigated for use in adaptive airframes [4–7] and robots [8,9] as well as potentially wind turbine blades [10–12] and automotive structures [13]. Moreover, it is possible to autonomously shape-morph these multi-stable composites by embedding active components such as piezoelectric (PZT) actuators [14–18] and shape memory alloy (SMA) wires [8,19]. In addition to morphing, vibration isolation [20] and energy harvesting [21,22] were also feasible with multi-stable composites. Compared to the equivalent linear systems that work ideally only near resonance frequencies, multi-stable composites perform well across a wider frequency bandwidth [23]. Such broadband advantage is especially evident when the laminates vibrate between their two stable states (aka. inter-well snap-through responses). Therefore, multi-stable composites are very promising lightweight and multi-functional structural systems.

However, it remains challenging to use these asymmetric fiber composites to obtain the complicated shapes changes and mechanical property adaptations that are required by many practical applications. The simplest asymmetric multi-stable composite—typically a rectangular patch with two different fiber angles through its thickness ([0°/90°] for example)—can only exhibit a cylinder-like shape at its stable states with free boundary conditions [3]. Such simplicity can severely limit the capability and performance of these composites. Therefore, it is crucial to incorporate design strategies to enrich their shape and performance. To this end, researchers have examined two strategies. The first involves assembly. For example, stacking multiple composite sheets together can create sandwich-like structures for controlled bending [11,24]; and connecting slender composite stripes can generate multi-stable lattices [25], tetrahedrons [26], and helical tubes [27]. The other strategy involves the careful design of the fiber layout in the laminate platform. That is, one can create sophisticated shape and mechanical property adaptations by introducing piece-wise [28–32], continuous [33,34], or tessellated [35,36] variations in fiber

* Corresponding author.
E-mail address: suyil@clemson.edu (S. Li).

https://doi.org/10.1016/j.compscitech.2019.107750
Received 13 May 2019; Received in revised form 19 July 2019; Accepted 21 July 2019
Available online 24 July 2019
0266-3538/

orientations. One can also embed initial curvatures during the curing process [37].

In this study, we propose a new strategy by inserting the principle of Kirigami cutting into the design of multi-stable composite structures, and introduce the concept of "Kirigami Composite". Kirigami is an ancient paper art with a simple yet powerful concept: One can cut a piece of paper according to a designated pattern, and then develop it into a sophisticated 3D shape by stretching and folding. Kirigami cutting has two unique properties that can help address the aforementioned challenge in multi-stable fiber composites. First, cutting makes it possible to achieve rich shape transformation. One of the most constraining factors regarding developing 2D sheets into 3D shapes is the continuity requirement. This constraint is most evident in the origami paper folding, which typically requires a very intricate crease pattern and essentially turns the paper into a kinematically over-constrained system. Cutting can effectively relax the continuity requirement and eliminate specific excessive constraints, thus offering extra mechanisms of shape reconfiguration that can be used to create mechanical metamaterials [38–40], multi-functional micro- and meso-structures [41–43], as well as robotic applications [44,45]. The second unique property of Kirigami is its versatility in manufacturing. Cutting is a reliable and scalable fabrication technique, so it is applicable to different materials with vastly different sizes: from one-atom thin graphene [46], nanocomposites [47], to macro-scale metals [41], polymer sheets [48], and electronic components [49,50]. Thus, it is possible to create cuttings easily in fiber composites using established fabrication tool and avoid excessive assembly.

To lay down the foundation for the design, fabrication, and analysis of Kirigami composite, this study focuses on its most elementary unit—a module consisting of a single slit cut and two bistable patches with carefully designed fiber arrangements (Fig. 1). This design is inspired by the Kirigami sheet with parallel cuts in a zig-zag fashion. We examine the multi-stability, snap-through, and potential applications of this multi-stable Kirigami composite module (simply referred to as "Kirigami module" hereafter) via extensive finite element simulations and experimental tests. Our results show that the Kirigami module can possess up to four stable states, and it exhibits snap-through instability due to a rapid "run-away" growth of surface curvature inversions from the connecting tab. These behaviors originate from the non-uniform connections between patches that are introduced by the cuts. We also show a stiffness adaptation function of the Kirigami module and how we can tailor its high/low stiffness ratio by customizing the cutting geometry. The following sections of this paper detail the design, fabrication, snap-through response, and stiffness adaptation of the Kirigami module.

2. Design and fabrication of Kirigami module

Design of the Kirigami module prototype is illustrated in Fig. 1 (b). This module consists of three layers of fiber laminates: 1) a base layer of [90°] fiber orientation; 2) a top layer of [0°] and 3) a bottom layer of [0°] fiber orientation. Dimensions of these layers (L_p, W_p) for the baseline design are listed in Table 1. A 100 mm long (L_c), 6 mm wide slit cut is made at the center of this module, essentially dividing it into two connected "patches" (Fig. 2). Since both patches feature the asymmetric [0°/90°] or [90°/0°] fiber ply arrangement, they are intended to be bistable. Here, we refer the structural connection between the two patches as the "connecting tab". This tab enforces a non-uniform connection between the two bistable patches which is examined extensively in the following studies regarding the external geometry, snap-through response, and stiffness adaptation of the overall Kirigami module.

We fabricate Kirigami module prototypes, according to the baseline design, using DA 409U/G35-150 carbon fiber prepregs embedded in HexPly 8552 resin. The fabrication procedure include three consecutive steps. The first step is freezing and cutting. The prepregs are cooled in a freezer to a temperature between 0 °C and 4 °C, and then they are cut according to the Kirigami module geometry using a paper cutter board or scissors. Freezing maintains the rigidity of the matrix resin so that the reinforcing carbon fibers in the prepregs would not be distorted during cutting. Any excessive distortions in fiber laminates can eliminate the desired multi-stability in finished prototypes. The second step of the fabrication is to assemble a vacuum bagging packet (Fig. 2(a)). A 0.6m × 0.6m × 4mm aluminum plate is used as the platform for this packet. This plate is covered with mold releasing agent, and the uncured Kirigami module samples are placed on its top. Then a layer of perforated plastic sheet (10 LYD 3015-PERF-D - Release Ply - High Temp 450F Perforated Film) is placed on top of the Kirigami module sample, followed by a polyester sheet (10 LYD 3000-D - Econo Ply J Polyester

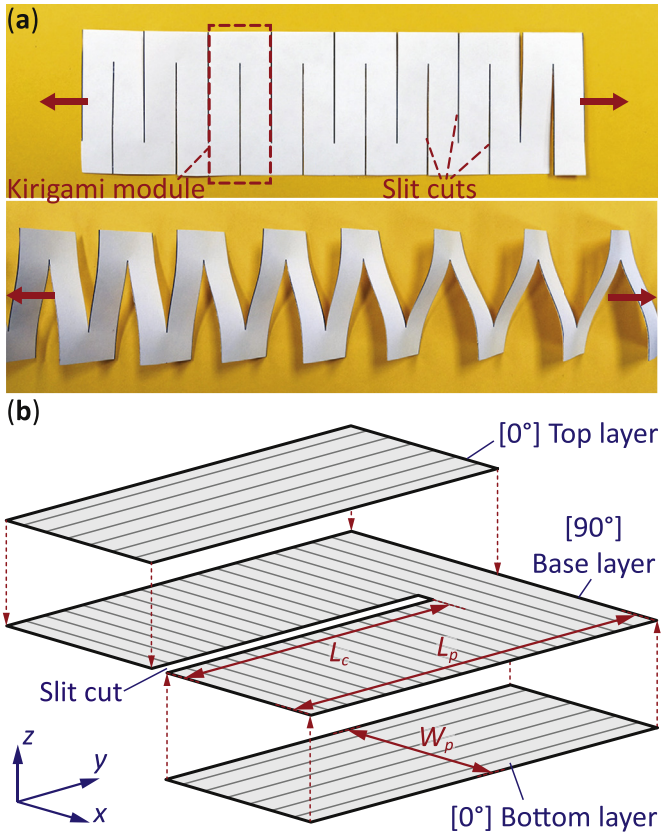

Fig. 1. Inspiration and the overall concept of the kirigami composite. (a): A paper kirigami featuring parallel slit cuts distributed in a "zig-zag" pattern. (b): The design of a multi- stable Kirigami composite module, which consists of two patches with asymmetric fiber arrangements. A slit cut is used to offer additional freedom to the patch deformation. Three cutting design parameters: patch length L_p, cut length L_c, and patch width W_p are highlighted here. Note that the patch width also represents the spacing in-between the parallel slit cuts if the module is assembled into a large Kirigami composite sheet.

Table 1
Baseline design parameters of the Kirigami module and its mechanical properties used in finite element simulations. Here, T_p is the thickness of Kirigami composite module.

Property	Value	Property	Value
L_p	130 mm	W_p	62 mm
L_c	100 mm	T_p	0.15 mm
E_1	135 GPa	G_{13}	7.17 GPa
E_2	9.5 GPa	G_{23}	3.97 GPa
ν_{12}	0.3	α_1	$-2 \times 10\text{-}8$ °C-1
G_{12}	5 GPa	α_2	$3.27 \times 10\text{-}5$ °C -1

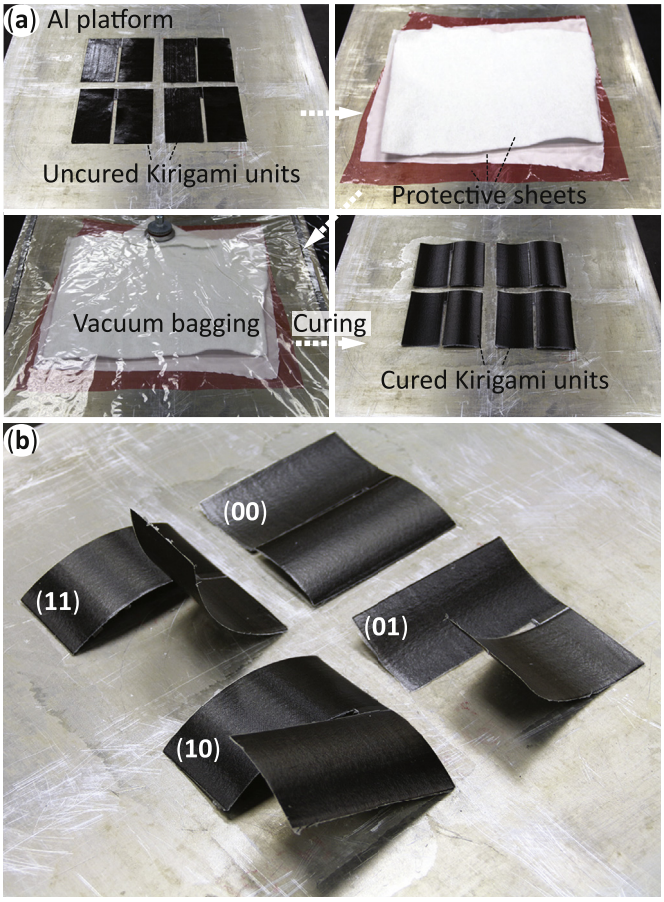

Fig. 2. Fabrication procedures of Kirigami module prototypes. (a) Photos showing the different steps of fabrication using the vacuum bagging method. (b) The finished prototypes show four different stable states. In this picture, Kirigami modules are switched between these stable states manually. Notice that the Kirigami module always settles into the (00) state after the curing and removing of the vacuum bagging.

Peel Ply). These layers are then covered with a sheet of absorbent material (10 LYD 3011-D - Breather Fabric). A nozzle is placed on top of this assembly and then it is sealed by vacuum bag films (10 LYD 3014-D - Stretchlon SL200 Vacuum Bag Film) and double-sided tapes. This entire packet is vacuumed using a VacuMaster 5 CFM Vacuum Pump. The third and final step of the fabrication is curing. The vacuum bagged packet is placed inside a heated oven at 135 °C for an hour, then it is cooled slowly down to the room temperature by turning off the oven. Such a heat-up and cool-down process induce internal thermal stresses in the laminates, which eventually result in the generation of bistability in both constituent patches (Fig. 2(b)).

After curing and removing the vacuum packet, it is found that both patches in the Kirigami module have already settled to one of their stable state as seen in the lower right picture of Fig. 2(a). We define this as the "initial (00)" state, where each number represents the configuration of one patch. Despite the kinematic constraints imposed by the connecting tab, the two constituent patches in the Kirigami module can exhibit bistablity *independently*. That is, if one patch is switched to a different stable state by an external force, the other patch can still stay at its initial state. In this way, the Kirigami module settles into either "(01)" or "(10)" state (Fig. 2(b)). Moreover, if both patches are switched away from its initial stable states, the Kirigami module settles into the "(11)" state.

3. External geometry at stable states

Fig. 3(a) shows the same fabricated Kirigami module as in Fig. 2, but square grid lines are drawn on its surface to better illustrate the external geometry. It is evident from this figure that both of the bistable patches take cylinder-like shapes, and the orientations of corresponding cylindrical longitudinal axis are different between different stable states. At the (0) state, the effective longitudinal axis is parallel to the length direction of the patch (or along the y-axis defined in Fig. 3(a)); while at the (1) state, the longitudinal axis is parallel to the patch width direction (or along the x-axis). The external shapes of the two constituent patches in Kirigami module are similar to the classical bistable patches with free boundary conditions [3], and this indicates that the kinematic constraints from connecting tab does not fundamentally alter the overall shapes of the asymmetric patches at their stable states. To accurately describe the external shape of Kirigami module, we place the fabricated sample in a NANOVEA™ST500 optical profilometer to measure its out-of-plane displacement and effective surface radius at different stable states (Fig. 3(c)). The measured radius along different edges and mid-sections of the patches are summarized in Table 2. It is worth highlighting that this experiment and all of the following ones are performed on this particular specimen to ensure consistency.

In parallel to the experimental study, we also develop a finite element model (FEM) for in-depth investigation and parametric studies. This model is developed in ABAQUS™software package using S4R thick shell element and nonlinear static solver (Fig. 3). The constitutive properties used in this finite element model are based on a very similar prepreg reported in previous literature [51,52], and they are listed in Table 2. The only exception is the thermal coefficient of expansion α_2, which can vary depending on the fabrication set up. We calibrated α_2 by matching the effective top-edge radius between the finite element predictions and profilometer readings. Overall, the finite element model can successfully re-produce the external shapes of the Kirigami module at different stable states without any significant discrepancies, and this model is used in the following studies.

4. Snap-through instability

Besides the external shapes at stable states, another important topic of examining multi-stable composites is their snap-through that occurs during the switch from one stable equilibrium to another. Snap-through of multi-stable composite has been studied using static [51,53–55] and dynamic [56–59] activations, and the boundary conditions are shown to play a central role. In the Kirigami module, the connecting tab imposes a complicated and non-uniform connection between the constituent patches. As a result, this tab can induce localized deformations and significantly affect the overall snap-through response. Therefore, we perform two studies to fully understand the snap-through in the Kirigami module by experimental tests and finite element simulation. The first study focuses on a single constituent patch, while the other focuses on the overall Kirigami module.

4.1. Single patch study

This study aims at understanding the snap-through instablity in a single bistable patch with the presence of connecting tab. In the experimental part of this study, we physically fix the connecting tab using a customized fixture, and apply a prescribed displacement along the z-axis at the free-end of the bistable patch using a universal tester machine (Fig. 4(a), ADMET eXpert 5000, 25N load cell). The end displacement increases at a 0.5 mm/s rate until the patch is switched from stable state (0) to state (1). Notice that in this experiment, the external load is applied to the Kirigami module prototype via a simple contact to accommodate the patch deformation along the y-axis. In other words, the rod from the tester overhead can slide on the patch surface.

Five tests are conducted on the bistable patch and the measured

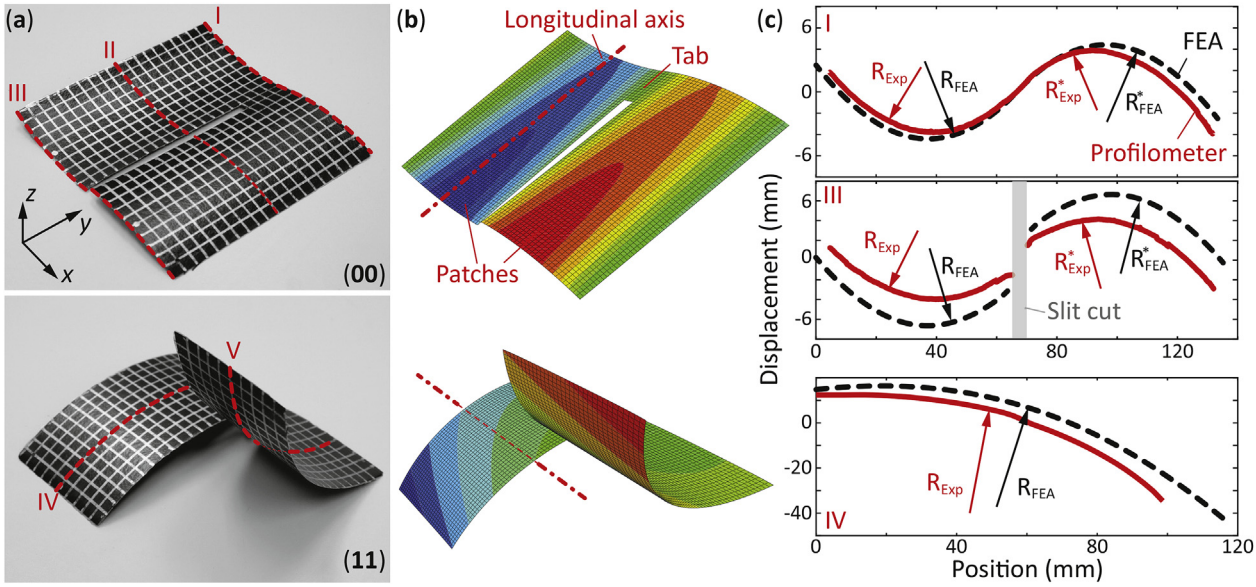

Fig. 3. The external shapes of the kirigami composite module at different stable states. (a) Close-up view of the Kirigami module with square grid-lines at the (00) and (11) state. The different curvatures shown in the grid-lines clearly show that the two constituent bistable patches take cylindrical shapes. Here, five cross-section curves (I, II, … V) are defined for profilometer readings. (b) Finite element simulations correctly reproduces the external shapes. Here the dot-dashed lines represent the effective longitudinal axes of the curved patches. (c) The out-of-plane displacements of three cross-section curves according to the profilometer readings and finite element simulations. Notice that for cross-section curves I, II, and III, two radius readings are obtained corresponding to the two constituent patches. Results of the curvature measurements are summarized in Table 2.

Table 2
Effective cylindrical radius of the bistable patches based on profilometer readings and finite element simulations. The locations of the five cross-sections are defined in Fig. 3(a). Notice that for cross-section curves I, II, and III, two radius readings are obtained corresponding to the two constituent patches.

Cross-section	R_{Exp}	R_{FEA}
I	104/101 mm	103/104 mm
II	99/101 mm	92/91 mm
III	120/112 mm	103/103 mm
IV	104 mm	103 mm
V	101 mm	104 mm

force-displacement relationships are shown in Fig. 4(b). Based on the results, it is evident that the switching from state (0) to state (1) consists of three consecutive stages. During the first stage, the reaction force increases, almost linearly, as the patch end displacement increases. This is due to the overall bending of the bistable patch. During the second stage, however, the reaction force starts to plateau even though the end displacement continue to increase significantly. A careful observation of composite patch reveals that during this stage, a localized "curvature inversion zone" started to originate and grow from the fixed tab. Within this zone, the initially curved grid lines along the *x*-axis becomes straight, and the initially straight grid lines along the *y*-axis becomes curved. Therefore, the corresponding surface curvature is inverted compared to the rest of the patch (Fig. 4(a,c)). Indeed, this curvature inversion is similar to what was observed from a single bistable patch subjected to a point force at its center [60]. As the patch end displacement increases, the boundary of such curvature inversion zone expands toward the opposite end of the bistable patch without significantly increasing the overall reaction force. It is worth emphasizing that in this second stage, if the end displacement were removed, the localized curvature inversion would disappear and bistable patch would return to its initial (0) state. In the last and final stage of switching, the snap-through or elastic instability finally occurs, and the boundary of curvature inversion zone quickly "propagates" throughout the rest of composite patch (Fig. 4(c) and Supplemental Video 1). As a result, the patch loses contact with the rod from the universal tester overhead, and snaps into stable state (1). Part of the excessive potential energy released in this stage is converted into structural vibration energy and then quickly damped out.

Supplementary video related to this article can be found at https://doi.org/10.1016/j.compscitech.2019.107750.

Therefore, the connecting tab in the Kirigami module induces a very unique, multi-staged response to the bistable patch when it is switched from state (0) to (1). The force-deformation curves obtained in finite element simulation confirms the experimental observation (Fig. 5). It is worth noting that, unlike the simple contact in the experiment, the patch end displacement in FEA is fully controlled (only in the *z*-axis). Therefore, there is a notable difference between FEA and experiment results regarding the magnitude of reaction force and displacement at different stages; and reaction force becomes negative after the occurrence of elastic instability: a classical response of a bistable structure with controlled displacement [23].

Moreover, we conduct additional finite element simulations of this state (0) to (1) switch based on different cut lengths L_c (Fig. 5(c and d)). If we increase the cut length (aka. shorter connecting tab), the distinction between stage 1 and 2 becomes subtle because the curvature inversion starts to develop very early. The magnitude of reaction force at the occurrence of stage 3 snap-through decreases but the corresponding end-displacement increases significantly. On the other hand, if the cut length is smaller (i.e. longer connecting tab), the initial stage 1 becomes more prominent and the corresponding reaction force increases significantly. This is because a longer connecting tab induces a larger curvature inversion zone, which requires a larger external force to develop. Moreover, we observe less of the state 2 growth of curvature inversion before the snap-through occurs. That is, the end-displacement corresponding to the stage 3 snap-through decreases. This is probably because a longer connecting tab reduces the energy barrier between the stable states (0) and (1). Indeed, if the cut length is further reduced to below half of the patch length ($L_c < 0.5L_p$), the two patches would lose their independent bi-stability and the module becomes a mono-stable structure.

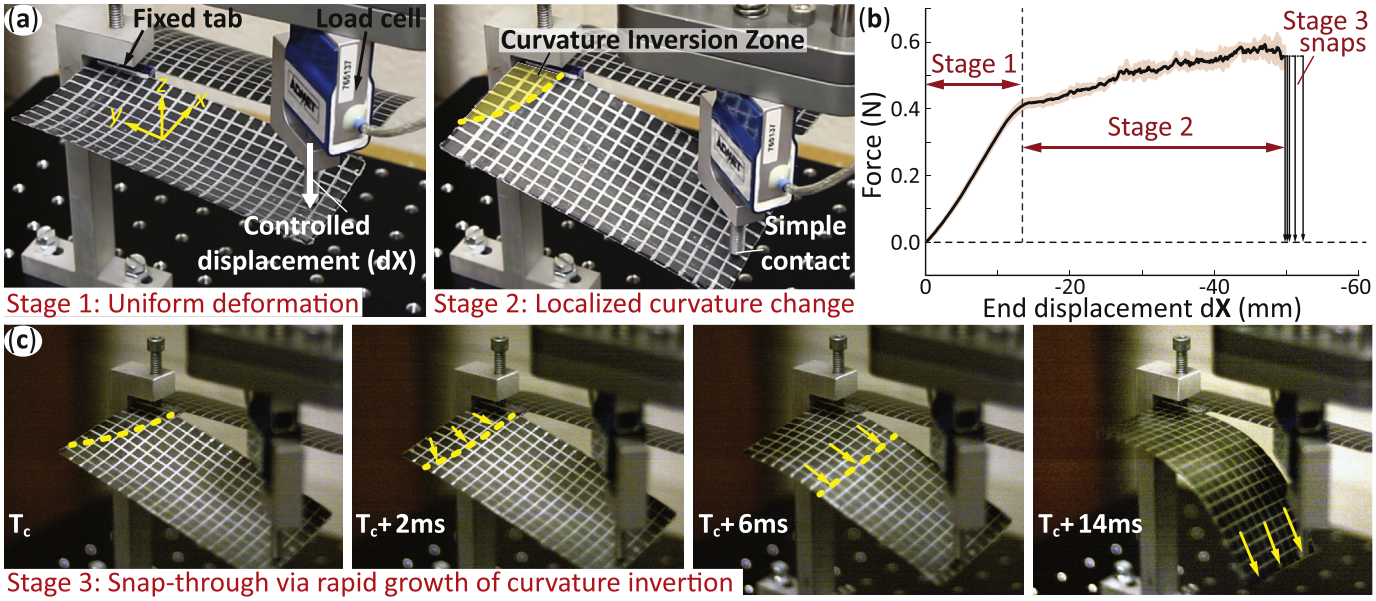

Fig. 4. Experiment observations of a constituent patch switching from stable state (0) to state (1) with the connecting tab fixed. (a) The experimental setup, also showing the deformation of the patch during stage 1 and 2 of the switching. The curvature inversion zone, which originates and grows from the fixed tab, is evident during the stage 2. (b) The measured force-displacement curves clearly shows the distinction between the three different stages. Five load cycles are applied; the black solid line and red shadow are the averaged reaction force and its standard deviation, respectively, during stage 1 and 2. The five arrows are the occurrence of snap-through instabilities (aka. the rapid "run-away" growth of the curvature inversion) in the five tests. The composite patch loses its contact with the universal tester overhead in stage 3, thus the reaction forces become zero. (c) High speed video footage of the stage 3 using a Photron Fastcam MINI UX-100 camera. T_c represents the critical time when the elastic instability occurs, and propagation of the front of curvature inversion zone is highlighted by the dashed curves. (For interpretation of the references to color in this figure legend, the reader is referred to the Web version of this article.)

4.2. Full Kirigami module study

This study aims to understand the snap-though behaviors in a complete Kirigami module as it is switched from (00) stable state to the (11) state. In this test, the free ends of the two constituent bistable patches are connected to the fixture and universal tester machine, respectively, through custom-made hinges (Fig. 6). In this way, controlled end displacement (dX) can be applied without inducing any constraints on patch rotation. Five load cycles are conducted on the Kirigami module prototype, and the measured force-displacement relationship is summarized in Fig. 6(b).

Two snap-through are observed in the test: the first occurs during

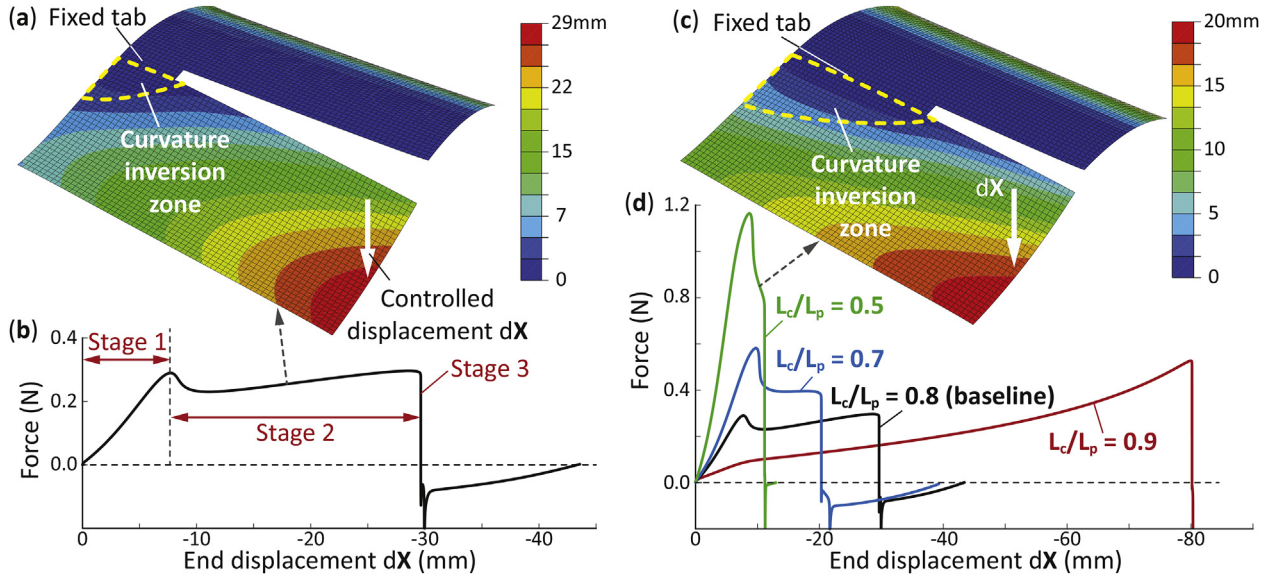

Fig. 5. Finite element simulation of a constituent patch switching from stable state (0) to state (1) with the connecting tab fixed. (a) Absolute nodal displacements during the stage 2 of switching using the same baseline designs as in the experiments, the higher stress in curvature inversion zone is evident. (b) Calculated force-displacement curve using the baseline design also shows a multi-staged response, which is qualitatively the same as experiment results show in Fig. 4. (c) Absolute nodal displacements in a Kirigami module with a shorter cut ($L_c = 0.5L_p$) right before the occurrence of stage 3 snap-through. (d) Force-displacement curves corresponding to different cut lengths. It is worth highlighting that in this and following figures, the color map in the finite element simulations represents the absolute nodal displacements with respect to the originally flat configuration *before curing*. (For interpretation of the references to color in this figure legend, the reader is referred to the Web version of this article.)

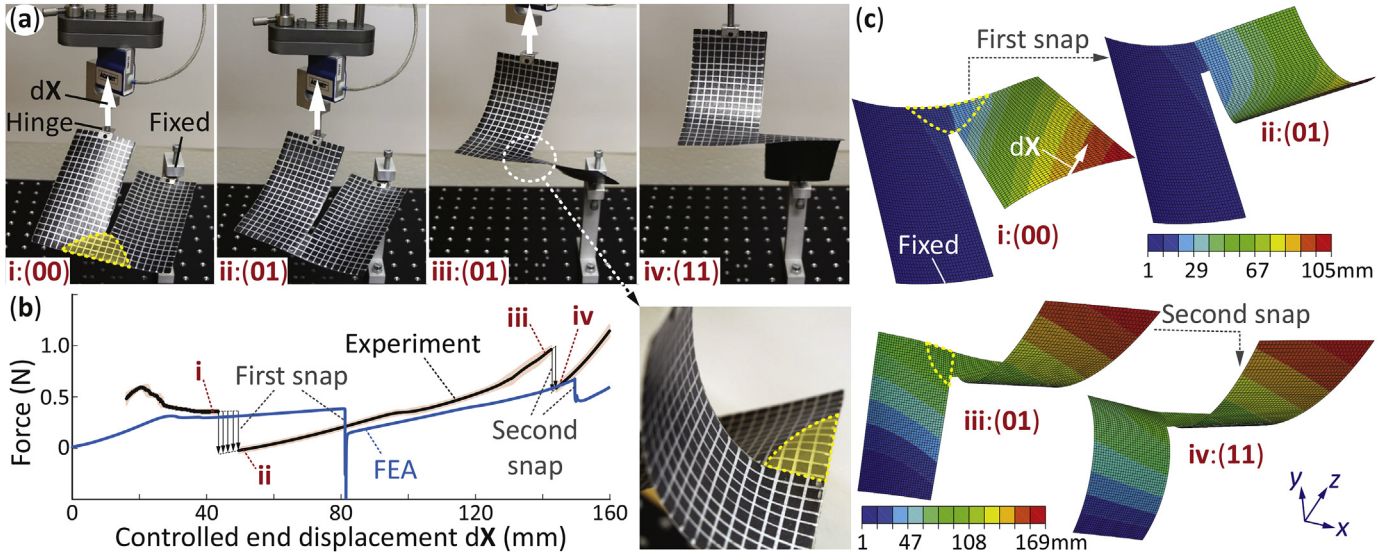

Fig. 6. Testing the snap-through in a complete Kirigami module. (a) Images of the Kirigami module at different configurations right before and after the two snap-through when it is switched from (00) to (01) and then (11) state. Curvature inversion zones are highlighted by the dashed lines. (b) The measured and predicted force-displacement curves. In the experimental results, the solid line is the averaged results, the shaded band is the standard deviation, and the arrows are the measured snaps in the five load cycles. The test data at very low end displacement shows excessive amount of variation due to gravity-induced sample rotation, so they are omitted for clarity. (c) Finite element simulations, showing the changes in nodal displacements before and after both snap-through. (For interpretation of the references to color in this figure legend, the reader is referred to the Web version of this article.)

the switch from (00) to (01) state, and the second during switch from (01) to (11). Before the occurrence of each snap-through, the two patches in the Kirigami module deform in a similar way as in the single patch study. That is, as the prototype is deformed from the initial (00) state to right before the first snap, curvature inversion zones originate from the connecting tab and grow into both bistable patches (configuration "i" in Fig. 6). However, right after the first snap-through, the curvature inversion zones disappear from both patches; One patch switches to stable state (1) and the other patch remained in stable state (0) (configuration "ii"). It is worth highlighting that the patch connected to the universal tester overhead always switches to stable state (1) first, thus the (10) state is never observed in this particular test. As the end displacement dX continues to increase, a new curvature inversion zone originates and grows into the patch that remained in state (0) (configuration "iii"). This zone again disappears after the second snap-through (configuration "iv"). Therefore, the presence of connecting tab plays a central role in the snap-through instability of Kirigami module as it is switched between different stable states, because it dictates generation of curvature inversion zone and load transfer between the two constituent patches. Understanding the mechanics underpinning these multi-staged switching and snap-through would be important for future practical implementations of the Kirigami composite concept.

The measured force-displacement curve qualitatively agrees with the numerical prediction based on the finite element, however, there is a notable discrepancy regarding the end displacement at the first snap-through. Given the sensitive nature of the elastically unstable snap-through, such a discrepancy can be a result of fabrication error and material property uncertainty, especially the laminate stiffness and thermal coefficient of expansion perpendicular to the fiber direction (aka. E_2 and α_2 in Table 1). In addition, the ambient humidity variation at the testing site plays a big role because when an asymmetric patch absorbs moisture, its residual stress from curing and the resulting bistability can be weakened significantly [61,62]. To reduce the negative effects of moisture ingress, the Kirigami module prototypes are re-heated in the oven at 135 °C for 15 min right before any tests (although this cannot completely eliminate the moisture issue). Moreover, there can be other sources of uncertainty such as chemical shrinkage and creep relaxation. Therefore, obtaining an accurate and quantitative agreement between finite element results and experiment measurements would require a substantial investigation into the process-property relationships of the asymmetric composite laminate, and this is beyond the scope of this study. Regardless, the discrepancy does not hinder us from understating the fundamental mechanics underpinning the snap-through instability in the Kirigami module, which is the focus of this paper.

5. Stiffness adaptation between stable states

A multi-stable structure or material system typically exhibits different mechanical properties at different stable states, and this creates opportunities to achieve on-demand mechanical property programming via strategically switching between these states [63–65]. To illustrate this capability in the Kirigami module, we investigate its effective stiffness at different stable states. In this study, the Kirigami module is stretched along the direction defined by its two free end corners as shown in Fig. 7(a and b). This loading condition is representative of the stretching of a multi-module Kirigami composite structure envisioned in Fig. 1(a). It is found that if the Kirigami module starts from (10) or (01) state, it would be quickly switched to the (11) state under such a stretching. However, if the Kirigami module is settled in either (00) or (11) state initially, the stretching would not trigger any switching between stable states. Therefore, we focus on the effective stiffness at the latter two states.

5.1. Origins of the stiffness adaptation

Fig. 7(a and b) show the external shapes of Kirigami module prototypes before and after stretching, and a close observation of these images reveals completely different deformation mechanisms between the (00) and (11) states. That is, if the Kirigami module starts from (00) state, the external stretch would only induce a concentrated twisting deformation near the connecting tab, while the majority of the two constituent bistable patches remain relatively un-deformed. This is because the cylindrical shapes of the bistable patches at the (00) states are orientated in a way that can effectively resist the external stretching

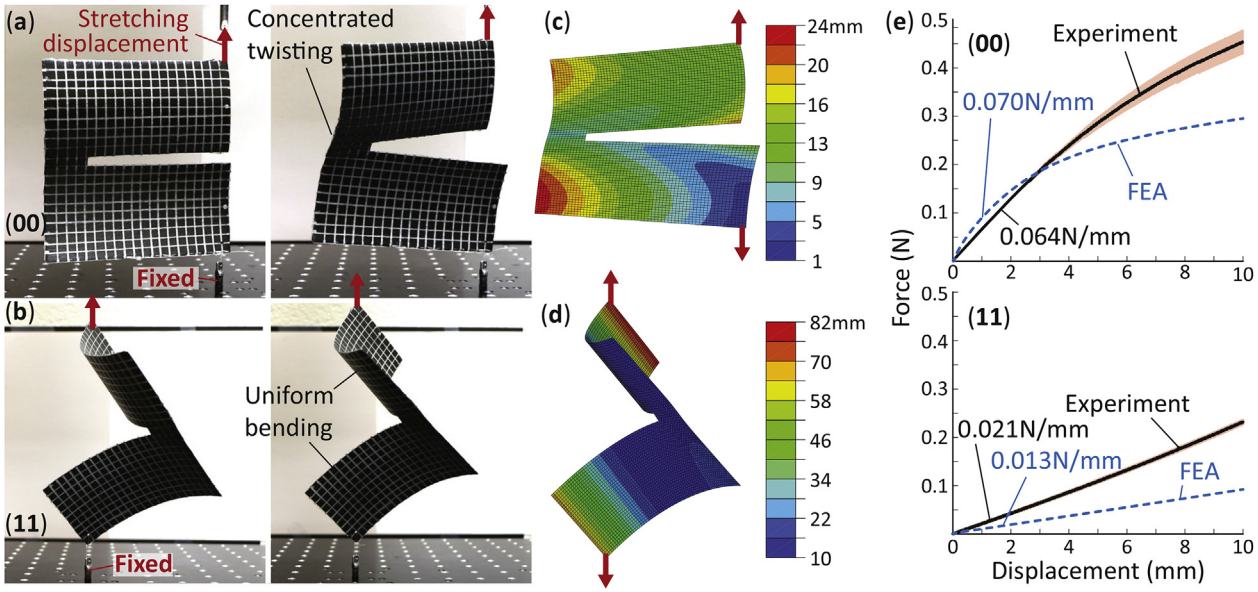

Fig. 7. Testing the effective stiffness of Kirigami composite module under a stretch between its two free end corners near the (00) and (11) stable states. (a, b): the experimental setup showing the external shape of the Kirigami module before and after the stretching. (c, d): The finite element simulation results showing the nodal displacement distributionwithin the Kirigami module. (e): A comparison between the measured and predicted reaction force-end displacement relationships. The solid curves are averaged experiment results, shaded bands are the standard deviation, and dashed curves are the results of finite element simulation.

force. Such a concentrated deformation is reflected by the finite element simulation (Fig. 7(c)). On the other hand, if the Kirigami module starts from the (11) state, the external stretch would instead induce a distributed bending deformation through out the patches. This is because the cylindrical shapes of the patches at this stable state are orientated in a way that does not resist the stretching deformation. As a result, the corresponding stress distribution, as predicted by the FEA (Fig. 7(d)), is more uniform compared to the case of (00) state.

Such fundamentally different deformation mechanisms between (00) and (11) states lead to notably different stiffness (Fig. 7(e)). The Kirigami module exhibits a relatively high and nonlinear stiffness near the (00) state due to the concentrated deformation near its connecting tab; but its effective stiffness is relatively low and mostly linear near the (11) state due to the more uniform deformation within its two patches. Finite element analyses and experimental results agree qualitatively regarding the deformation mechanism and overall reaction force-displacement relationship. However, they show a discrepancy regarding the magnitude of reaction force. Near the (00) state, the measured reaction force exceeds the finite element prediction; while near the (11) state, the measured force is below the finite element prediction. Here, we estimated the effective stiffness by performing a linear regression on the force-displacement curve over the 0 mm–2 mm displacement range. The measured and simulated stiffness near the (00) state are 0.064N/mm and 0.070N/mm, respectively. The corresponding stiffness near the (11) state are 0.021N/mm and 0.013N/mm, respectively.

As discussed in the previous section, these discrepancies in magnitude probably originate from fabrication error, material property variations, and ambient humidity. Regardless, experiment results and finite element simulation together confirm the physical principles behind the stiffness adaptation of the Kirigami composite module.

5.2. Tailoring the stiffness adaptation

A unique advantage of the Kirigami composite is that the underlying principle of cutting is geometric, so we have a large freedom to tailor the overall structural performance by customizing the cutting pattern. Here, we use the finite element model to examine the relationship between the cutting geometry and stiffness ratio, which is defined as the ratio of the effective stiffness near the (00) stable state over the (11) state:

$$R_K = \frac{K_{(00)}}{K_{(11)}}. \tag{1}$$

Two design parameters are considered in this parametric study: one is the length of the cut L_c (Fig. 8); and the other is the width of the constitutive bistable patch W_p, which is representative for the spacing between the parallel slit cuts in this Kirigami design. Moreover, both cut length and patch width are normalized by the patch length (L_p).

Finite element simulation results in Fig. 8(a) shows a strong correlation between the magnitudes of module stiffness and cutting design parameters. Near the (00) stable state, a shorter cutting length L_c (aka. a longer connecting tab) generally corresponds to a higher stiffness $K_{(00)}$. This is because the connecting tab is primarily contributing to the overall stiffness at the (00) state, indicated by the results shown in Fig. 7. On the other hand, the correlation between $K_{(11)}$ and cutting length is not as strong. This is because the bistable constituent patches contribute to the overall stiffness the most near the (11) state. As a result, for the same patch width W_p, shorter cut length L_c leads to higher stiffness ratio R_K (Fig. 8(b)). However, if the cut is too short (aka. $L_c/L_p < 0.5$), the kinematic constraints imposed by the resulting long connecting tab can cause the constituent patches to lose their independent bistablity. As a result, the overall Kirigami composite no longer exhibit the four unique stable states shown in Fig. 2, and the stiffness ratio can no longer be property defined. Therefore, the stiffness ratio reaches its maximum shortly before the independent patch bistabiliy is lost.

For the same cut length L_c, a smaller patch width W_p generally gives a higher stiffness ratio (R_K) (Fig. 8(b)). This is because reducing the patch width would reduce the overall module stiffness near the (11) stable state, but increase the stiffness near the (00) state. Overall, this parametric study confirms the potential of tailoring the stiffness adaption performance by customizing the slit cut length and spacing. Results of such parametric studies can be used for formulating a design methodology that can distribute the cutting pattern according to a prescribed stiffness adaption performance.

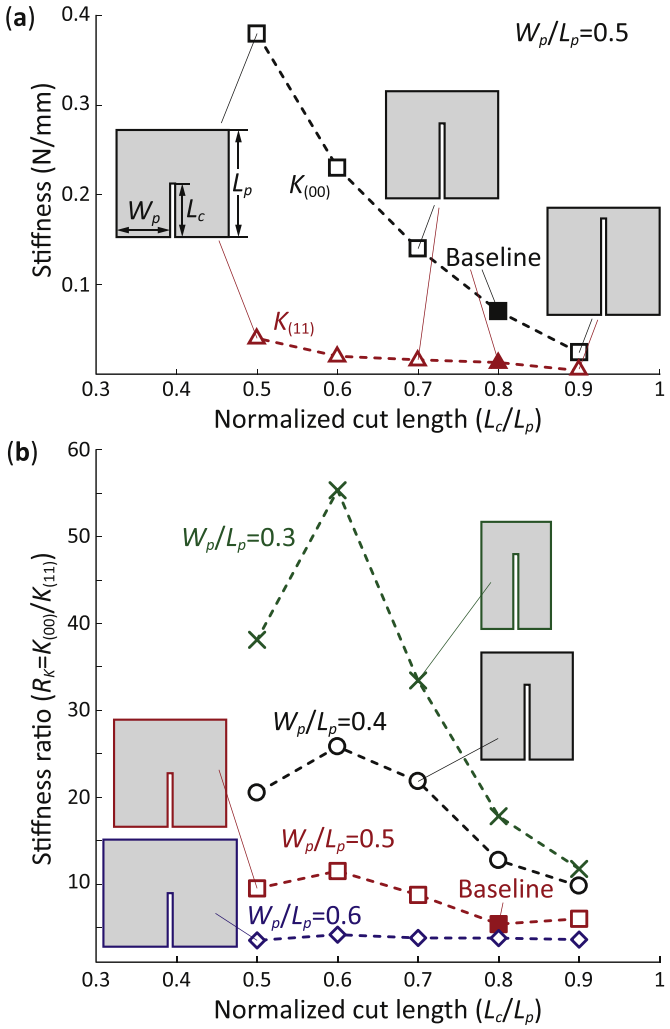

Fig. 8. Parametric study based on the finite element simulations. (a) The correlations between the normalized cutting length L_c/L_p and the magnitudes of module stiffness ($K_{(00)}$, $K_{(11)}$). (b) The correlations between the cutting geometries and the stiffness ratio (R_K). The baseline design used throughout this study is highlighted. Notice that the constituent patches lose their individual bistability when $L_c/L_p < 0.5$.

6. Summary and discussion

This study proposes and examines an adaptive Kirigami composite concept by applying the art of Kirigami cutting into multi-stable composite laminates with asymmetric fiber layout. Specifically, we focused on the snap-through instability and stiffness adaptation of an elementary module in the Kirigami composite in order to lay down the foundation of understanding the mechanics and performance of this new structural concept. This module consists of two bistable patches connected via a connecting tab, and the length of this tab is directly related to the cut length. Because the cutting can relax kinematic constraints between the constituent bistable patches, the Kirigami module overall exhibits four unique stable states.

The connecting tab imposes a complex, non-uniform connection between the two constituent bistable patches, as a result, the Kirigami composite module exhibits a unique snap-though that can be best described as a multi-staged creation, growth, and "run-away" propagation of surface curvature inversion zones. Such curvature inversion originates from the connecting tab, and the bistable patch switch between stable states via the rapid propagation of curvature inversion. Both experimental observations and finite element simulations confirm such unique snap-through, which are crucial for the practical implementation and control of the multi-stable Kirigami composites.

Moreover, we experimentally and numerically demonstrated an effective stiffness adaptation function by switching the Kirigami composite module between its (00) and (11) stable states. Such a stiffness variation originates from the fundamentally different shapes and deformation mechanisms of the Kirigami module between its stable states. The effective stiffness ratio of (00) state over the (11) state is strongly correlated to the cutting pattern design parameters, such as the cut length and the spacing between the parallel cuts. This opens up the opportunely to customize-design the a large-scale Kirigami composite consisting of many patches and slit cuts in order to achieve a on-demand stiffness programming with prescribed performance.

7. Data availability

The raw and processed data to reproduce these findings are available upon request.

Acknowledgement

The authors thank Dr. Georges Fadel at Clemson University for many fruitful discussions. A. Lele and V. Deshpande acknowledge the financial support from Clemson University. S. Li also acknowledge the support from National Science Foundation (Award # CMMI-1633952, 1751449 CAREER, and 1760943). O. Myers acknowledge the support from Clemson University.

Appendix A. Supplementary data

Supplementary data to this article can be found online at https://doi.org/10.1016/j.compscitech.2019.107750.

References

[1] M.W. Hyer, Some observations on the cured shape of thin unsymmetric laminates, J. Compos. Mater. 15 (1981) 175–194.
[2] M.W. Hyer, The room-temperature shapes of four-layer unsymmetric cross-ply laminates, J. Compos. Mater. 16 (1982) 318–340.
[3] S.A. Emam, D.J. Inman, A review on bistable composite laminates for morphing and energy harvesting, Appl. Mech. Rev. 67 (2015) 060803.
[4] S. Daynes, P.M. Weaver, Stiffness tailoring using prestress in adaptive composite structures, Compos. Struct. 106 (2013) 282–287.
[5] A.F. Arrieta, I.K. Kuder, M. Rist, T. Waeber, P. Ermanni, Passive load alleviation aerofoil concept with variable stiffness multi-stable composites, Compos. Struct. 116 (2014) 235–242.
[6] S. Daynes, P. Weaver, J. Trevarthen, A morphing composite air inlet with multiple stable shapes, J. Intell. Mater. Syst. Struct. 22 (2011) 961–973.
[7] J. Sun, Q. Guan, Y. Liu, J. Leng, Morphing aircraft based on smart materials and structures: a state-of-the-art review, J. Intell. Mater. Syst. Struct. 27 (2016) 2289–2312.
[8] S.W. Kim, J.S. Koh, J.G. Lee, J. Ryu, M. Cho, K.J. Cho, Flytrap-inspired robot using structurally integrated actuation based on bistability and a developable surface, Bioinspiration Biomimetics 9 (2014) 036004.
[9] Z. Zhang, D. Chen, H. Wu, Y. Bao, G. Chai, Non-contact magnetic driving bioinspired Venus flytrap robot based on bistable anti-symmetric CFRP structure, Compos. Struct. 135 (2016) 17–22.
[10] M.R. Schultz, A concept for airfoil-like active bistable twisting structures, J. Intell. Mater. Syst. Struct. 19 (2008) 157–169.
[11] C.G. Diaconu, P.M. Weaver, F. Mattioni, Concepts for morphing airfoil sections using bi-stable laminated composite structures, Thin-Walled Struct. 46 (2008) 689–701.
[12] X. Lachenal, S. Daynes, P.M. Weaver, Review of morphing concepts and materials for wind turbine blade applications, Wind Energy 16 (2013) 283–307.
[13] S. Daynes, P.M. Weaver, Review of shape-morphing automobile structures: concepts and outlook, Proc. Inst. Mech. Eng. - Part D J. Automob. Eng. 227 (2013) 1603–1622.
[14] M.R. Schultz, M.W. Hyer, Snap-through of unsymmetric cross-ply laminates using piezoceramic actuators, J. Intell. Mater. Syst. Struct. 14 (2003) 795–814.
[15] A.F. Arrieta, O. Bilgen, M.I. Friswell, P. Hagedorn, Dynamic control for morphing of bi-stable composites, J. Intell. Mater. Syst. Struct. 24 (2013) 266–273.
[16] M. Gude, W. Hufenbach, C. Kirvel, Piezoelectrically driven morphing structures based on bistable unsymmetric laminates, Compos. Struct. 93 (2011) 377–382.
[17] D.V. Murray, O.J. Myers, Modeling bistable composite laminates for piezoelectric morphing structures, ISRN Mater. Sci. 2013 (2013) 1–12.
[18] D.V. Murray, O.J. Myers, Modeling fiber composites during the cure process for

piezoelectric actuation, World J. Mech. 03 (2013) 26–42.
[19] M.L. Dano, M.W. Hyer, SMA-induced snap-through of unsymmetric fiber-reinforced composite laminates, Int. J. Solids Struct. 40 (2003) 5949–5972.
[20] A.D. Shaw, S.A. Neild, D.J. Wagg, P.M. Weaver, A. Carrella, A nonlinear spring mechanism incorporating a bistable composite plate for vibration isolation, J. Sound Vib. 332 (2013) 6265–6275.
[21] A.F. Arrieta, P. Hagedorn, A. Erturk, D.J. Inman, A piezoelectric bistable plate for nonlinear broadband energy harvesting, Appl. Phys. Lett. 97 (2010) 104102.
[22] D.N. Betts, H.A. Kim, C.R. Bowen, D.J. Inman, Optimal configurations of bistable piezo-composites for energy harvesting, Appl. Phys. Lett. 100 (2012) 114104.
[23] R.L. Harne, K.W. Wang, A review of the recent research on vibration energy harvesting via bistable systems, Smart Mater. Struct. 22 (2013) 023001.
[24] S. Daynes, P.M. Weaver, K.D. Potter, Aeroelastic study of bistable composite airfoils, J. Aircr. 46 (2009) 2169–2174.
[25] F. Dai, H. Li, S. Du, A multi-stable lattice structure and its snap-through behavior among multiple states, Compos. Struct. 97 (2013) 56–63.
[26] M. Santer, S. Pellegrino, Compliant multistable structural elements, Int. J. Solids Struct. 45 (2008) 6190–6204.
[27] A. Pirrera, X. Lachenal, S. Daynes, P.M. Weaver, I.V. Chenchiah, Multi-stable cylindrical lattices, J. Mech. Phys. Solids 61 (2013) 2087–2107.
[28] F. Mattioni, P.M. Weaver, M.I. Friswell, Multistable composite plates with piecewise variation of lay-up in the planform, Int. J. Solids Struct. 46 (2009) 151–164.
[29] A.F. Arrieta, I.K. Kuder, T. Waeber, P. Ermanni, Variable stiffness characteristics of embeddable multi-stable composites, Compos. Sci. Technol. 97 (2014) 12–18.
[30] K.D. Potter, P.M. Weaver, A concept for the generation of out-of-plane distortion from tailored frp laminates, Compos. Appl. Sci. Manuf. 35 (2004) 1353–1361.
[31] W. Jiang, M. Li, Y. Yao, F. Dai, Design of a multistable composite laminate by variable cross-section method and applying the displacement constraint, Mater. Des. 147 (2018) 35–47.
[32] Y. Cui, M. Santer, Highly multistable composite surfaces, Compos. Struct. 124 (2015) 44–45.
[33] C.S. Sousa, P.P. Camanho, A. Suleman, Analysis of multistable variable stiffness composite plates, Compos. Struct. 98 (2013) 34–46.
[34] P.M. Anilkumar, A. Haldar, E. Jansen, B.N. Rao, R. Rolfes, Design optimization of multistable variable-stiffness laminates, Mech. Adv. Mater. Struct. 26 (2019) 48–55.
[35] Y. Cui, M. Santer, Characterisation of tessellated bistable composite laminates, Compos. Struct. 137 (2016) 93–104.
[36] A.S. Panesar, P.M. Weaver, Optimisation of blended bistable laminates for a morphing flap, Compos. Struct. 94 (2012) 3092–3105.
[37] S. Mostafavi, M. Golzar, A. Alibeigloo, On the thermally induced multistability of connected curved composite plates, Compos. Struct. 139 (2016) 210–219.
[38] Y. Cho, J.H. Shin, A. Costa, T.A. Kim, V. Kunin, J. Li, S.Y. Lee, S. Yang, H.N. Han, I.S. Choi, D.J. Srolovitz, Engineering the shape and structure of materials by fractal cut, Proc. Natl. Acad. Sci. 111 (2014) 17390–17395.
[39] A. Rafsanjani, K. Bertoldi, Buckling-induced kirigami, Phys. Rev. Lett. 118 (2017) 084301.
[40] Y. Tang, G. Lin, S. Yang, Y.K. Yi, R.D. Kamien, J. Yin, Programmable kiri-kirigami metamaterials, Adv. Mater. (2016) 1604262.
[41] Y. Zhang, Z. Yan, K. Nan, D. Xiao, Y. Liu, H. Luan, H. Fu, X. Wang, Q. Yang, J. Wang, W. Ren, H. Si, F. Liu, L. Yang, H. Li, J. Wang, X. Guo, H. Luo, L. Wang, Y. Huang, J.A. Rogers, A mechanically driven form of Kirigami as a route to 3D mesostructures in micro/nanomembranes, Proc. Natl. Acad. Sci. 112 (2015) 11757–11764.
[42] Z. Yan, F. Zhang, J. Wang, F. Liu, X. Guo, K. Nan, Q. Lin, M. Gao, D. Xiao, Y. Shi, Y. Qiu, H. Luan, J.H. Kim, Y. Wang, H. Luo, M. Han, Y. Huang, Y. Zhang, J.A. Rogers, Controlled mechanical buckling for origami-inspired construction of 3D microstructures in advanced materials, Adv. Funct. Mater. 26 (2016) 2629–2639.
[43] R. Neville, A. Monti, K. Hazra, F. Scarpa, C. Remillat, I. Farrow, Transverse stiffness and strength of Kirigami zero-ν PEEK honeycombs, Compos. Struct. 114 (2014) 30–40.
[44] H. Shigemune, S. Maeda, Y. Hara, U. Koike, S. Hashimoto, Kirigami robot: making paper robot using desktop cutting plotter and inkjet printer, IEEE/RSJ International Conference on Intelligent Robots and Systems (IROS), IEEE, 2015, pp. 1091–1096.
[45] K. Zhang, C. Qiu, J.S. Dai, Helical kirigami-enabled centimeter-scale worm robot with shape-memory-alloy linear actuators, J. Mech. Robot. 7 (2015) 021014.
[46] M.K. Blees, A.W. Barnard, P.A. Rose, S.P. Roberts, K.L. McGill, P.Y. Huang, A.R. Ruyack, J.W. Kevek, B. Kobrin, D.A. Muller, P.L. McEuen, Graphene kirigami, Nature 524 (2015) 204–207.
[47] T.C. Shyu, P.F. Damasceno, P.M. Dodd, A. Lamoureux, L. Xu, M. Shlian, M. Shtein, S.C. Glotzer, N.A. Kotov, A kirigami approach to engineering elasticity in nanocomposites through patterned defects, Nat. Mater. 14 (2015) 785–789.
[48] K. Saito, S. Pellegrino, T. Nojima, Manufacture of arbitrary cross-section composite honeycomb cores based on origami techniques, J. Mech. Des. 136 (2014) 051011.
[49] A. Lamoureux, K. Lee, M. Shlian, S.R. Forrest, M. Shtein, Dynamic kirigami structures for integrated solar tracking, Nat. Commun. 6 (2015) 8092.
[50] Z. Song, X. Wang, C. Lv, Y. An, M. Liang, T. Ma, D. He, Y.J. Zheng, S.Q. Huang, H. Yu, H. Jiang, Kirigami-based stretchable lithium-ion batteries, Sci. Rep. 5 (2015) 10988.
[51] P. Portela, P. Camanho, P. Weaver, I. Bond, Analysis of morphing, multi stable structures actuated by piezoelectric patches, Comput. Struct. 86 (2008) 347–356 (Smart Structures).
[52] A. Fernandes, C. Maurini, S. Vidoli, Multiparameter actuation for shape control of bistable composite plates, Int. J. Solids Struct. 47 (2010) 1449–1458.
[53] M.-L. Dano, M.W. Hyer, Thermally-induced deformation behavior of unsymmetric laminates, Int. J. Solids Struct. 35 (1998) 2101–2120.
[54] M.-L. Dano, M. Hyer, SMA-induced snap-through of unsymmetric fiber-reinforced composite laminates, Int. J. Solids Struct. 40 (2003) 5949–5972.
[55] M.R. Schultz, M.W. Hyer, Snap-through of unsymmetric cross-ply laminates using piezoceramic actuators, J. Intell. Mater. Syst. Struct. 14 (2003) 795–814.
[56] A.F. Arrieta, O. Bilgen, M.I. Friswell, P. Hagedorn, Dynamic control for morphing of bi-stable composites, J. Intell. Mater. Syst. Struct. 24 (2013) 266–273.
[57] O. Bilgen, A.F. Arrieta, M.I. Friswell, P. Hagedorn, Dynamic control of a bistable wing under aerodynamic loading, Smart Mater. Struct. 22 (2013) 025020.
[58] M.S. Taki, R. Tikani, S. Ziaei-Rad, A. Firouzian-Nejad, Dynamic responses of cross-ply bi-stable composite laminates with piezoelectric layers, Arch. Appl. Mech. 86 (2016) 1003–1018.
[59] A.F. Arrieta, D.J. Wagg, S.A. Neild, Dynamic snap-through for morphing of bi-stable composite plates, J. Intell. Mater. Syst. Struct. 22 (2011) 103–112.
[60] K. Potter, P. Weaver, A.A. Seman, S. Shah, Phenomena in the bifurcation of unsymmetric composite plates, Compos. Appl. Sci. Manuf. 38 (2007) 100–106.
[61] C.J. Brampton, D.N. Betts, C.R. Bowen, H.A. Kim, Sensitivity of bistable laminates to uncertainties in material properties, geometry and environmental conditions, Compos. Struct. 102 (2013) 276–286.
[62] J. Etches, K. Potter, Weaver, I. Bond, Environmental effects on thermally induced multistability in unsymmetric composite laminates, Compos. Appl. Sci. Manuf. 40 (2009) 1240–1247.
[63] J. Meaud, K. Che, Tuning elastic wave propagation in multistable architected materials, Int. J. Solids Struct. 122–123 (2017) 69–80.
[64] R.L. Harne, Z. Wu, K.W. Wang, Designing and harnessing the metastable states of a modular metastructure for programmable mechanical properties adaptation, J. Mech. Des. 138 (2015) 021402.
[65] J.N. Grima, R. Caruana-Gauci, M.R. Dudek, K.W. Wojciechowski, R. Gatt, Smart metamaterials with tunable auxetic and other properties, Smart Mater. Struct. 22 (2013) 084016.